SPACE WEATHER, VOL. 7, S12001, doi:10.1029/2009SW000468, 2009

Minimum variance analysis-based propagation of the solar wind observations: Application to real-time global magnetohydrodynamic simulations

A. Pulkkinen[1,2] and L. Rastätter[2,3]

Received 30 January 2009; revised 6 July 2009; accepted 3 October 2009; published 2 December 2009.

[1] The performance of the bulk of the current real-time space weather applications is dependent on the accuracy of the driver solar wind data. One of the central aspects associated with the accuracy of the driver data is the determination of the propagation delay time of single-spacecraft solar wind observations from Lagrangian point L1 to the Earth. In this work, the value of the minimum variance analysis-based solar wind propagation technique as applied to real-time global magnetohydrodynamic (MHD) simulations is investigated. Both the method that uses the newly introduced technique for minimizing the effect of the poorly determined phase planes and the minimum variance analysis-based setup by Weimer and King (2008) along with the standard simple convection delay-based (no phase planes used) solar wind propagation technique are applied to global MHD-based modeling of the ground magnetic field and geomagnetically induced current variations. All computations are carried out in a real-time setting. It is shown by means of comparisons to ground-based observations that while the minimum variance analysis-based propagation techniques can be used to optimize the timing associated with the propagated solar wind fluctuations, the improvement is so modest that from the statistical viewpoint, the benefit over using the simpler propagation technique vanishes for the studied storm period when the information is passed through real-time global MHD modeling process.

Citation: Pulkkinen, A., and L. Rastätter (2009), Minimum variance analysis-based propagation of the solar wind observations: Application to real-time global magnetohydrodynamic simulations, *Space Weather*, *7*, S12001, doi:10.1029/2009SW000468.

1. Introduction

[2] The importance of accurate determination of propagation delay time of single-spacecraft solar wind observations from halo orbit around Lagrangian point L1 to the Earth has been addressed and debated recently in a series of papers by *Weimer et al.* [2002, 2003], *Bargatze et al.* [2005], *Haaland et al.* [2006], *Bargatze et al.* [2006], *Weimer and King* [2008], and *Mailyan et al.* [2008]. More specifically, the cited papers studied the minimum variance analysis-based solar wind propagation technique that identifies and utilizes orientations of the phase planes in the interplanetary medium. The subject is potentially of great importance for single-spacecraft L1-based space weather applications as depending on the method used to propagate the observations, prediction timing errors up to tens of minutes may result [*Weimer et al.*, 2002, 2003]. Ten minutes is obviously substantial in comparison to the lead time (typically 30 to 60 min) given by L1-based observations.

[3] *Pulkkinen et al.* [2007] recently introduced a global magnetohydrodynamic (MHD) based approach to modeling of ground magnetic field and geomagnetically induced current (GIC) variations. The approach has been utilized in the Community Coordinated Modeling Center (CCMC) operated at NASA Goddard Space Flight Center to experimentally forecast GIC in different nodes of the North American high-voltage power transmission system. CCMC's real-time GIC estimates are a part of the "Solar Shield" project funded by NASA Applied Sciences program and carried out in collaboration with the Electric Power Research Institute. Optimization of the experimental GIC forecasting system, whose performance is strongly dependent on the accuracy of the input solar wind data, is one of the main components of Solar Shield. Consequently, the main motivation of the paper at hand is to test if the phase plane–based propagation (the terms "minimum variance analysis-based propagation" and "phase plane–based propagation" will be used interchangeably throughout the paper) of the solar wind observations can provide significant improvement to the accuracy of the

[1]Goddard Earth Sciences and Technology Center, University of Maryland Baltimore County, Baltimore, Maryland, USA.
[2]NASA Goddard Space Flight Center, Greenbelt, Maryland, USA.
[3]Department of Physics, Catholic University of America, Washington, D. C., USA.

global MHD-based real-time ground magnetic field and GIC modeling. If a major improvement is obtained, it would be a clear indication that L1-based space weather forecasts should adopt the more advanced solar wind propagation technique over the simple convection delay approach that ignores the varying orientations of the phase planes. The test will be carried out here by driving a global MHD model with the propagated solar wind observations and by using the ionospheric output of the model to predict the magnetic field and GIC at different locations on the surface of the Earth. Because the most significant space weather effects are associated with strong or extreme events, the model chain will be driven for the time period containing the Halloween storm events of October 2003. It is emphasized that in contrast to recent efforts by *Weimer and King* [2008] and *Mailyan et al.* [2008], a single but long and continuous time period instead of a collection of discontinuity events is analyzed and the propagated solar wind data is used in a MHD modeling process in a fashion applicable to real-time space weather computations. It should be noted that isolated discontinuity events form only one element of the wide class of interplanetary drivers of geomagnetic activity. From the GIC-related space weather applications viewpoint, continuous time periods covering more general interplanetary conditions should be treated in evaluating the propagation methods.

[4] Much of the earlier debate cited above originated from a fortunate programming error made by *Weimer et al.* [2003], which resulted in a method that was able to accurately estimate the propagation delays. More specifically, instead of regular minimum variance analysis of the magnetic field fluctuations, *Weimer et al.* [2003] carried out a constrained minimum variance analysis finding minimum variance planes (approximately) perpendicular to the mean magnetic field direction [*Bargatze et al.*, 2005; *Haaland et al.*, 2006; *Bargatze et al.*, 2006]. *Bargatze et al.* [2005] and *Haaland et al.* [2006] suggested that the method should be corrected to find the plane exactly perpendicular to the mean magnetic field and showed how this can be done. For completeness, it will be shown below that the methods suggested by *Bargatze et al.* [2005] and *Haaland et al.* [2006] are mathematically equivalent. Further, a novel method for stabilizing the phase planes in real-time application of the minimum variance analysis-based solar wind propagation will be introduced, optimized and tested.

[5] The structure of the paper is as follows. In the Appendix, the mathematics needed for the standard and constrained minimum variance analysis are reviewed. In Section 2 a new method for stabilizing the fluctuations in the determined phase planes is introduced. In Section 3 the techniques from the previous sections are combined and optimal values for the two free parameters of the novel solar wind propagation approach are determined. For comparison, the optimization of the minimum variance-based propagation setup by *Weimer and King* [2008] is also studied. Finally, in Section 4 the introduced approach along with the *Weimer and King* [2008] setup will be applied to the period of 24 October to 1 November 2003 to study if the phase plane–based propagation method improves the accuracy of the ground magnetic field and GIC predictions. In Section 5 each step of the solar wind propagation approach discussed and further developed in this paper is summarized and concluding remarks on different solar wind propagation techniques are given.

2. Technique for Stabilizing the Phase Plane Orientations

[6] Sometimes data does not allow for a good and unique determination of a phase plane. In these occasions large and undesirable fluctuations in the determined phase plane orientations occur (see Figure 1). *Weimer et al.* [2003] and *Weimer and King* [2008, and references therein] discuss the rules used to disregard the ''bad'' phase planes by means of criteria for the ratios of the eigenvalues associated with the minimum variance system and limits for the acceptable orientations of the planes (these rules are referred below shortly as the *Weimer and King* [2008] setup). The selection of the acceptable ratios and orientations increases the number of free parameters of the propagation method and completely disregarding apparently bad phase planes may generate undesirable effects in real-time applications where interpolations between the well-determined planes cannot be carried out. One such effect is locking on to some specific phase plane orientation for extended time periods (see Figure 1). An alternative technique, having only one free parameter to adjust, for stabilizing the phase plane orientations is thus introduced.

[7] The fundamental assumption of the new technique is that a large fraction of the computed phase planes are well determined. Thus, one only wants to minimize the effect of the poorly determined planes on the overall temporal evolution of the phase plane orientations. To do this, one introduces inertia to the evolution of the phase planes in terms of equation

$$m\frac{d\mathbf{n}}{dt} = -\nabla V(|\mathbf{n} - \mathbf{n}^*|) \tag{1}$$

where m is the ''mass'' (units in seconds) of the plane dictating how slowly the orientation of the phase plane reacts to the force acting on it. The force on the right-hand side of equation (1) is defined as a gradient of potential $V(|\mathbf{n} - \mathbf{n}^*|)$, which is dependent on the distance between the modeled phase plane normal and the normal $\mathbf{n}^*$ predicted by the minimum variance analysis. By introducing an additional layer of modeling one can control sudden and possibly erroneous changes in the orientations of the phase planes.

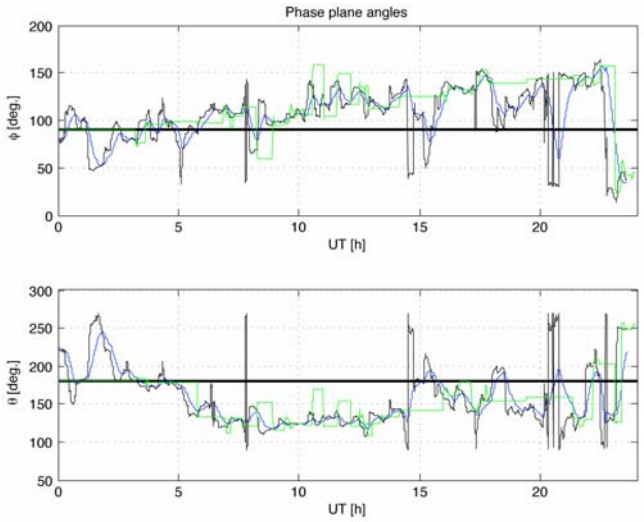

Figure 1. Phase plane normal **n** orientations as a function of time. Here ϕ is the polar angle, and θ is the azimuthal angle in the spherical GSE coordinate system (**n** having ϕ = 90° and θ = 180°, shown with the thick black lines, points toward the Earth). The thin black line shows the orientations without the stabilization, the blue line shows the orientations when the stabilization is used, and the green line shows the orientations obtained by using the *Weimer and King* [2008] setup. In using the stabilized method, the length of the analysis window is 25 min, and the "mass" m of the stabilized plane is 30 min. In using the *Weimer and King* [2008] setup, the cutoff ratio of 7.8, the limiting angle of 75 degrees between the solar wind velocity and the phase plane, and the analysis window length of 6.25 min were used. The time is UT hours from the beginning of 2 July 1999. ACE MAG data interpolated to 15 s time resolution was used to determine the phase planes.

[8] For simplicity, the potential $V(|\mathbf{n} - \mathbf{n}^*|)$ is selected to be a quadratic potential well:

$$V(\mathbf{n}) = |\mathbf{n} - \mathbf{n}^*|^2 \tag{2}$$

The predicted **n*** will define the bottom of the potential well in equation (2) toward which the phase plane normal following equation (1) tends to. By using the first order forward difference expansion of equation (1), one obtains a rule for updating the phase plane normals:

$$\mathbf{n}(t_{j+1}) = \mathbf{n}(t_j) + \frac{2}{m}\left(\mathbf{n}^* - \mathbf{n}(t_j)\right)\Delta t \tag{3}$$

where $\Delta t = t_{j+1} - t_j$. Note that once equation (3) has been applied, the normal needs to be renormalized; that is, condition $|\mathbf{n}(t_{j+1})| = 1$ has to hold.

[9] Figure 1 shows an example how the method stabilizes the phase plane orientations for the 24 hour period of 2 July 1999. It is emphasized that the locking to some specific phase plane orientations in Figure 1, in contrast to similar analysis by *Weimer and King* [2008], is caused by the real-time setting of the analysis: interpolations between the well-determined planes cannot be carried out. The calculations associated with Figure 1 are discussed more in detail in the next section.

[10] In summary, the approach introduced here for carrying out the phase plane–based propagation of the solar wind observations is applied as follows: 1.) the data is analyzed in overlapping analysis windows. The magnetic field fluctuations perpendicular to the mean field within each window is analyzed by using the minimum variance analysis and the eigenvectors $\mathbf{v}_i$ of the data covariance matrix in equation (A7) are determined. 2.) The predicted phase plane normal **n*** is $\mathbf{v}_i$ associated with the intermediate eigenvalue λ_i. If the x component (GSM or GSE) of **n*** is positive, **n*** = $-$**n*** is computed; that is the normal is forced to point toward the Earth. 3.) The normal **n** is propagated according to equation (3) by using the phase plane mass m. 4.) The time delay corresponding to the data in the window is computed by using the formula

$$\tau = \frac{\mathbf{n} \cdot (\mathbf{r}_2 - \mathbf{r}_1)}{\mathbf{n} \cdot \langle \mathbf{V}_{sw} \rangle} \tag{4}$$

where $\mathbf{r}_1$ is the location from which data is propagated, $\mathbf{r}_2$ the location to which data is propagated and $\langle \mathbf{V}_{sw} \rangle$ the mean velocity of the solar wind within the analysis window. 5.) Solar wind data in the first time step of the window (in real-time computations this corresponds to "now") is propagated by using the corresponding τ. 6.) The process is repeated in overlapping windows, in the increments of the resolution of the data, until the entire time series has been treated. 7.) The propagation will produce data in nonuniform temporal resolution and interpolation is used to bring the data back into a uniform temporal grid. Note that the interpolation will automatically deal with data points that "overtake" earlier time steps. Interpolation was found to be better approach in comparison to disregarding the overtaking (or lagging) data points also by *Weimer and King* [2008].

3. Optimal Setup for the Propagation

[11] The novel approach for propagating the solar wind observations has two free parameters that need to be set prior to computations. Namely, one has to choose the length of the analysis window used to determine **n*** via minimum variance analysis and the mass used to stabilize the temporal evolution of the phase plane orientations. There are no obvious rules for fixing these parameters and thus it is of interest to study if the values can be chosen in some optimal way, as was suggested by *Sonnerup and Scheible* [1998].

[12] Magnetic field (B_x, B_y, B_z) and solar wind velocity (v_x, v_y, v_z) data from Advanced Composition Explorer (ACE) and Geotail for i) 2 July 1999 00:00–24:00 UT and for ii) 24 September 1998 08:00 UT to 25 September 1998 08:00 UT are used in the computations. The two periods were chosen based on the two different solar wind states associated with them: while period i was associated with highly fluctuating interplanetary magnetic field, it was not associated with strong geomagnetic activity (the minimum Dst index of the period was −23 nT) and period ii was associated with a strong geomagnetic storm, the minimum Dst of the period being −202 nT. The mean location (x, y, z in GSE) of ACE for the period i was (237, 39, −1) R_E and of Geotail (23, 19, −1) R_E and for the period ii (243, −30, 13) R_E and (18, −23, −2) R_E, respectively. The mean velocity of the solar wind at ACE for the period i was (−600, −26, −25) km/s and for the period ii (−571, 8, 20) km/s. First, both ACE and Geotail data were interpolated to a 15 s temporal resolution. Then ACE magnetic field and solar wind velocity data were propagated to the Geotail location by using the novel approach and the window length used in the minimum variance analysis and the mass of the phase planes used in the stabilization of the phase planes were varied systematically to cover the parameter space of interest. For comparison, phase planes were determined also by using the *Weimer and King* [2008] setup. In this case, instead of mass of the phase plane, the cutoff ratio $\lambda_{max}/\lambda_{int}$ of maximum and intermediate eigenvalues associated with the minimum variance system was varied, and following *Weimer and King* [2008], if the angle between the solar wind velocity and the phase plane exceeded 75 degrees, the phase plane was disregarded. In disregarding a bad phase plane, the previous well-determined plane was used. It is noted again that in real-time applications of the *Weimer and King* [2008] setup, one cannot interpolate between the well-determined phase planes as this would require knowledge about the future orientations of the phase planes. The optimal parameters for both approaches are the ones that give the best correspondence between Geotail magnetic field and solar wind velocity and the propagated ACE magnetic field and solar wind velocity.

[13] It is quite reasonable to assume that large scale interplanetary structures retain their spatiotemporal signatures while propagating from the ACE to the Geotail location. In contrast, localized small-scale fluctuations cannot be expected to retain their structure over large interplanetary distances. It follows that exclusion of the small-scale fluctuations from the parameter optimization is desirable as their inclusion may cause smearing of the better correlated features at larger scales. Accordingly, coherence between two signals $h(t)$ and $g(t)$ defined as

$$c_{hg}(f) = \frac{|HG|^2}{|H|^2|G|^2} \quad (5)$$

where f denotes frequency and upper case letters denote quantities in the spectral domain will be used to measure the correspondence between the signals. It is noted that the coherence as defined in equation (5) is related to the correlation coefficient in the time domain via the cross-correlation theorem. The mean coherence $\langle c_{hg} \rangle$, the mean being taken over only certain frequencies to exclude the small-scale features from the analysis, will be computed below.

[14] Figures 2 and 3 show the mean coherence taken over the periods of 10–512 min and over different magnetic field and solar wind velocity components (coherence was computed separately for each magnetic field and velocity component) as functions of the length of the analysis window, the mass of the phase plane and the cutoff ratio. The choice of using periods between 10 and 512 min to compute $\langle c_{hg} \rangle$ is quite arbitrary. However, the central features discussed below are relatively robust and were observable also when the mean was taken, for example, over the periods of 5–512 min (not shown).

[15] Interestingly, as is seen from Figures 2a and 3a, there is a clearly identifiable linear relationship between the optimal values of the length of the analysis window and the mass of the phase plane up to window lengths of about 30 min. This suggests the two parameters are not independent but linked via the approximate relation $y = 1.2\,x$. The relationship effectively renders the number of free parameters in the introduced approach to only one, the analysis window length. No similar dependence between the optimal values of the length of the analysis window and the cutoff ratio can be identified from Figures 2b and 3b where the optimal setups are seen to be distributed for the period i within cutoff ratio of about 1–8 and analysis window length of about 2–11 min and for the period ii 1–6 and 15–39 min, respectively. The optimal parameters for the *Weimer and King* [2008] setup thus seems to vary greatly from period to period making the choice of the universally optimal parameters problematic. It is noted that the optimal range of values for the period i is in rough agreement with the results by *Weimer and King* [2008] who found that the cutoff ratio of 7.8 and the window length of 6.25 min provides one of the optimal setups for the solar wind propagation.

[16] The above analysis was carried out also for the simple convection delay method, the maximum mean coherence being in this case 0.40 and 0.53 for the periods i and ii, respectively. On the contrast, in Figures 2 and 3 both analyses provide maximum coherences of 0.52 and 0.56 for the periods i and ii, respectively. Consequently, while the novel approach based on the stabilized phase planes and the approach based on the *Weimer and King* [2008] setup performed with similar accuracy, the phase plane–based propagation improved the accuracy of the propagation of the solar wind from the ACE to the Geotail location for the studied periods.

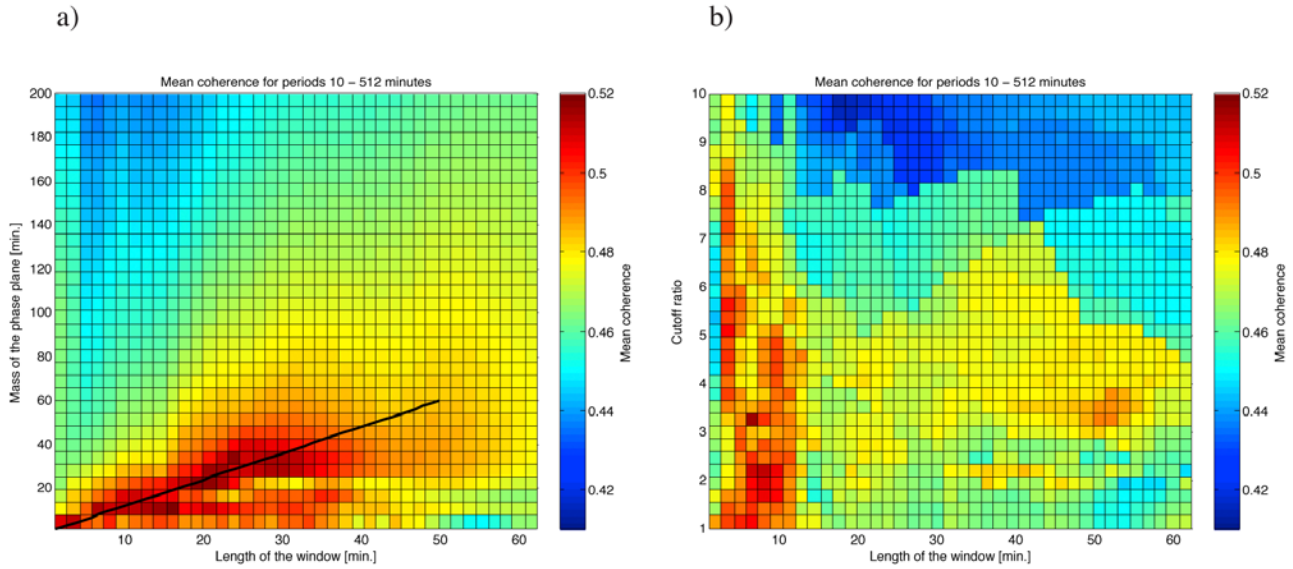

Figure 2. (a) Mean coherence between the propagated and the observed magnetic field and solar wind velocity fluctuations for the period i as functions of the length of the analysis window and the mass of the phase plane. The thick black line shows a linear model of the form $y = 1.2 \cdot x$. (b) Mean coherence between the propagated and the measured magnetic field and solar wind velocity fluctuations for the period i as functions of the length of the analysis window and the cutoff ratio used in the *Weimer and King* [2008] setup. In both Figures 2a and 2b the coherence is the mean taken over different magnetic field and solar wind velocity components and frequencies indicated above the plots. See text in Section 3 for details.

[17] Finally, it is noted that although the analysis associated with the novel propagation approach indicated possible existence of optimal parameters valid for varying solar wind states, the analysis above is strictly valid only for the studied two time periods; generalizations to other situations would require a comprehensive analysis of a data set representing large collection of different solar wind conditions.

4. Application of the Propagation Procedure

[18] In this section the value of the phase plane–based propagation over the simple convection delay propagation

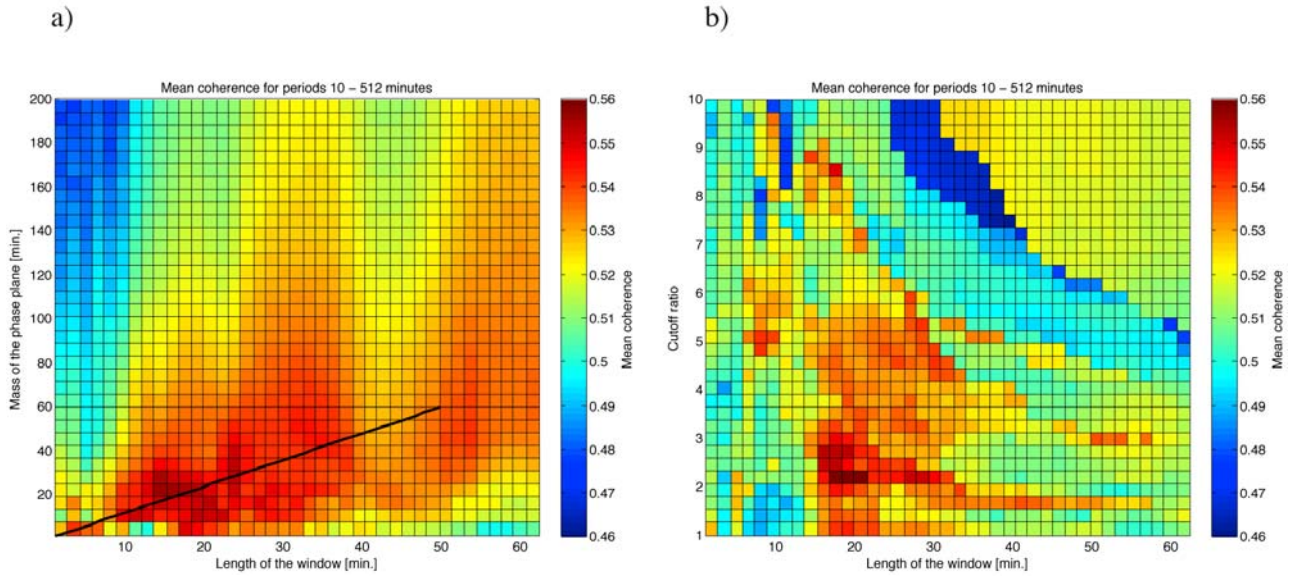

Figure 3. Same as Figure 2 but for the period ii.

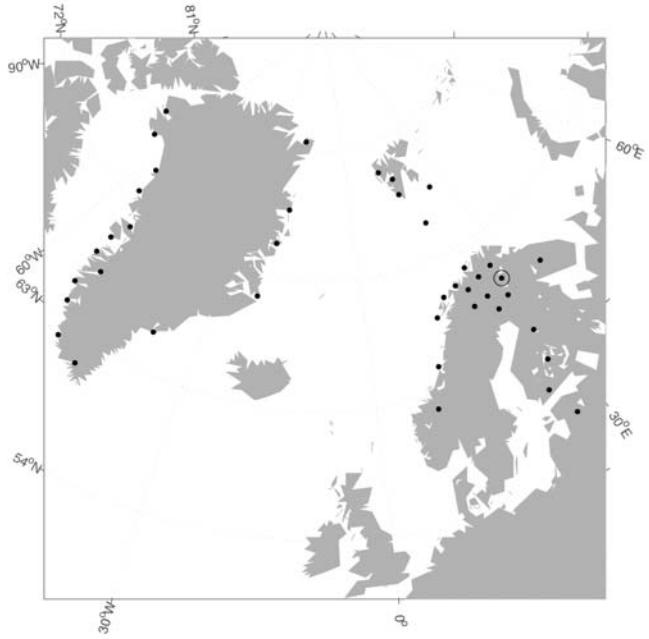

Figure 4. The locations of the Greenland and IMAGE magnetometer stations used in the study. The open circle indicates the location of the station used to compute GIC in Figure 6. Geographic coordinates are used.

of the solar wind data is evaluated. The application of interest is the global MHD-based calculation of the ground magnetic field and geomagnetically induced current (GIC) (for more on GIC, see, e.g., *Boteler et al.* [1998] and *Molinski* [2002]). The modeling is carried out by using Block-Adaptive-Tree-Solarwind-Roe-Upwind-Scheme (BATS-R-US) global MHD model driven with solar wind observations and the ground magnetic field and GIC are computed to the locations of the Greenland and International Monitor for Auroral Geomagnetic Effects (IMAGE) magnetometer stations (Figure 4). The modeling process is identical to that by *Pulkkinen et al.* [2007] and is composed of the following steps: 1) propagated solar wind is used to drive BATS-R-US, 2) BATS-R-US ionospheric output is used as an input to the Complex Image Method (CIM) [*Pirjola and Viljanen*, 1998] that is used to compute the external and internal components of the ground magnetic field at given locations. CIM also provides the ground electric field. In step 3), the computed ground electric field is used with the given system parameters (depending on the topological and electrical characteristics of the technological conductor system) to map the CIM output into GIC values at given locations. Note that geomagnetic field observations can be used with the system parameters to calculate the ''observed'' GIC to which modeled MHD-based GIC can be compared to. For details of the modeling process, reader is referred to *Pulkkinen et al.* [2007]. The only difference to the MHD setup by *Pulkkinen et al.* [2007] is that instead of a minimum cell width of 0.5 R_E, a minimum cell width of 0.25 R_E is used, which resulted in about 500.000 global MHD model cells.

[19] The ACE magnetic field and plasma data by *Skoug et al.* [2004] for the period of 24 October to 1 November 2003 are used to generate the boundary conditions for MHD model computations. Note that the period contains the Halloween storm events of 29–31 October 2003. The mean location (x, y, z in GSE) of ACE for the period was (231.5, 40.9, −20.9) R_E and the spacecraft was thus well off the Sun-Earth line. The mean velocity of the solar wind at ACE for the period was (−732, −10, 4) km/s. The modeling process is then repeated identically for three cases: a) ACE observations propagated to the MHD model boundary at (33, 0, 0) R_E (GSM), by using the simple convection delay, i.e., propagation time computed by dividing the distance by the average (over analysis windows) of the x component of the solar wind velocity, b) ACE observations propagated to the MHD model boundary by using the stabilized phase planes as described in the sections above and c) ACE observations propagated to the MHD model boundary by using the *Weimer and King* [2008] setup. Using the results from Section 3, in b) the analysis window length of 25 min and phase plane mass of 30 minutes and in c) the analysis window length of 6.25 min and the cutoff ratio of 7.8 consistent with the optimal parameters found by *Weimer and King* [2008] were chosen to be used. The circumsolar motion of the Earth that causes a slight shift in the location of the target was not taken into account in the propagation calculations. It should be noted that due to the extreme nature of the Halloween event, especially ACE plasma density observations contain significant inaccuracies for the part of the modeled time period. However, as all model runs contain the same inaccuracies, the presence of partly inaccurate density data is not expected to alter the central results of the analysis.

[20] Figures 5, 6, and 7 show the interplanetary magnetic field propagated to the MHD model boundary, GIC modeled to one of the magnetometer stations and *IE* index, local variant of the *AE* index computed from the modeled and the measured magnetic field at Greenland and IMAGE stations, for the beginning of the Halloween storm events. This time period is of special interest as forecasting the start time of extreme disturbances accurately is of great importance from the space weather applications viewpoint.

[21] From Figure 5 it can be seen that different propagation techniques do provide shifted solar wind magnetic field at the MHD model boundary. More specifically, between 06:00 and 06:30 UT the stabilized phase plane–based magnetic field precedes the simple convection delay-based field by about three minutes and *Weimer and King* [2008] setup–based field precedes the former by about five minutes. By looking at Figure 6 it is seen that the shifts are in the correct direction: the actual observed GIC disturbance starts at about 06:07 UT, which quite well

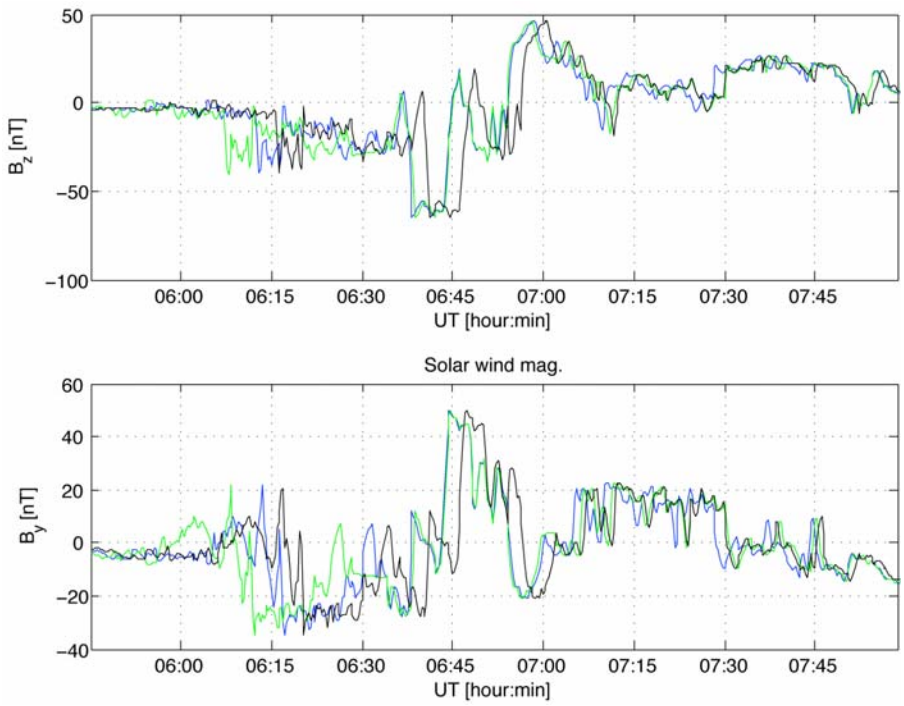

Figure 5. The (a) z and (b) y components (GSM) of the solar wind magnetic field propagated to (33, 0, 0) R_E. The black lines in both Figures 5a and 5b indicate the field propagated using the simple convection delay, the blue lines show the field propagated using the phase planes with the stabilization, and the green lines show the field obtained by using the *Weimer and King* [2008] setup. The time is UT hours of 29 October 2003.

matches the timing of the disturbance obtained by using the *Weimer and King* [2008] setup. The same conclusion holds also for the magnetic field fluctuations as can be observed from Figure 7. Thus, it is seen that for the beginning of the Halloween storm events, the phase plane–based techniques do improve the timing associated with the solar wind input fed into the MHD model.

[22] One intriguing feature observable from Figures 5–7 is that relatively small differences in MHD input generate very large differences in the ground magnetic field and especially in GIC behavior. This clearly is a manifestation of the highly nonlinear nature of the modeled solar wind-magnetosphere-ionosphere system. The sensitivity of the global MHD models to inflow boundary conditions is a poorly studied subject and the observation made here calls for further investigations on the subject. The subject has implications also on the best achievable modeling accuracy: small observational uncertainties in the MHD inflow conditions may be amplified, for example, into large uncertainties in the ionospheric output.

[23] A more rigorous statistical analysis of the modeled GIC for the period of 24 October to 1 November 2003 was carried out by means of the utility metric that measures the model's capability to reproduce events. Shortly, in applying the utility metric one identifies crossings of given GIC thresholds, i.e., events, within forecast windows that are slid over both the observed and the modeled data. One then identifies "hits" and "false alarms" of the forecasts and computes, for example, the forecast ratio R_f, which is the ratio hits over false alarms, to quantify the model performance. Thus, greater forecast ratios in Figure 8 indicate better model performance. The details of the application of the metric to the setting of interest are given by *Pulkkinen et al.* [2007]. Here, however, the utility was calculated separately by using both nonoverlapping and overlapping forecast windows that were slid over the modeled and the observed data sets. In using the overlapping forecast windows, the windows were moved in steps of the temporal resolution of the data, i.e., in 4 minute increments.

[24] The results of the utility analysis are shown in Figure 8. It is seen that while the analysis with independent forecast windows cannot show any clear difference between the utilities associated with different solar wind propagation techniques, the usage of overlapping forecast windows does indicate greater utility for the phase plane–based modeled GICs at greater GIC event amplitudes. This improvement is, however, a consequence of individual large peak in GIC on 29 October at about 06:45 UT (see Figure 6), which was captured better by the phase plane–

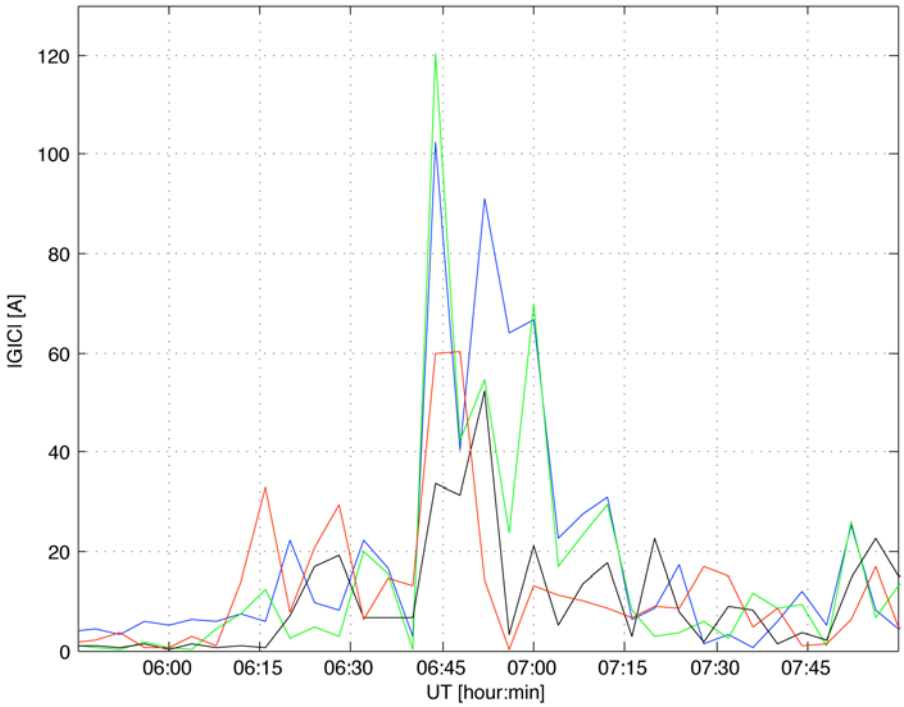

Figure 6. The absolute value of GIC modeled to one of the auroral stations indicated in Figure 4. The red curve shows the "measured" GIC based on the observed ground magnetic field (for detailed discussion in this, see *Pulkkinen et al.* [2007]). The black line indicates modeled GIC obtained using the simple convection delay, the blue line indicates modeled GIC obtained using the phase planes with the stabilization, and the green line shows modeled GIC obtained by using the *Weimer and King* [2008] setup. The time is UT hours of 29 October 2003.

based modeled GICs. We thus conclude that from the utility metric viewpoint, neither of the phase plane–based solar wind propagation techniques provide systematic improvement in the GIC modeling accuracy for the studied time period.

[25] To see if the above conclusion holds also for the modeled magnetic field fluctuations, the prediction efficiencies *PE* for the derived *IE* indices were computed. *PE* is defined as

$$PE = 1 - \frac{\langle (IE_{obs} - IE_{mod})^2 \rangle}{\sigma_{obs}^2} \quad (6)$$

where IE_{obs} and IE_{mod} are the observed and the modeled signals, respectively, and σ_{obs}^2 is the variance of the observed signal. Note that $PE = 1$ indicates a perfect prediction while $PE = 0$ means that the model predicts the signal equally well to the mere mean value of the signal. *IE* modeled for the period of 24 October to 1 November 2003 by using the stabilized phase planes gives $PE = 0.31$, *IE* modeled by using the *Weimer and King* [2008] setup gives $PE = 0.30$ and *IE* modeled by using the simple convection delay gives $PE = 0.30$. Thus, also from the viewpoint of the modeled magnetic field fluctuations, the phase plane–based propagation techniques do not provide clear statistical improvement over the simple convection delay propagation technique for the studied time period.

5. Conclusions

[26] In this work, minimum variance analysis-based solar wind propagation techniques identifying and utilizing orientation of the phase planes in the interplanetary medium were investigated. The mathematical relation between different approaches appearing in the literature was clarified and a new technique for minimizing the effect of poorly determined phase planes was introduced. Importantly, the new approach adopted here for determining and modeling the evolution of the phase planes has only two free parameters that can in principle be optimized. The optimization was carried out by utilizing ACE and Geotail magnetic field and solar wind velocity observations for the periods of 2 July 1999 00:00–24:00 UT and 24 September 1998 08:00 UT to 25 September 1998 08:00 UT. Interestingly, the analysis revealed that the two free parameters of the new approach are not independent but there is, for reasons that warrant further investigation, an identifiable linear relationship between the two over the given range of values. Thus, in effect, the method has

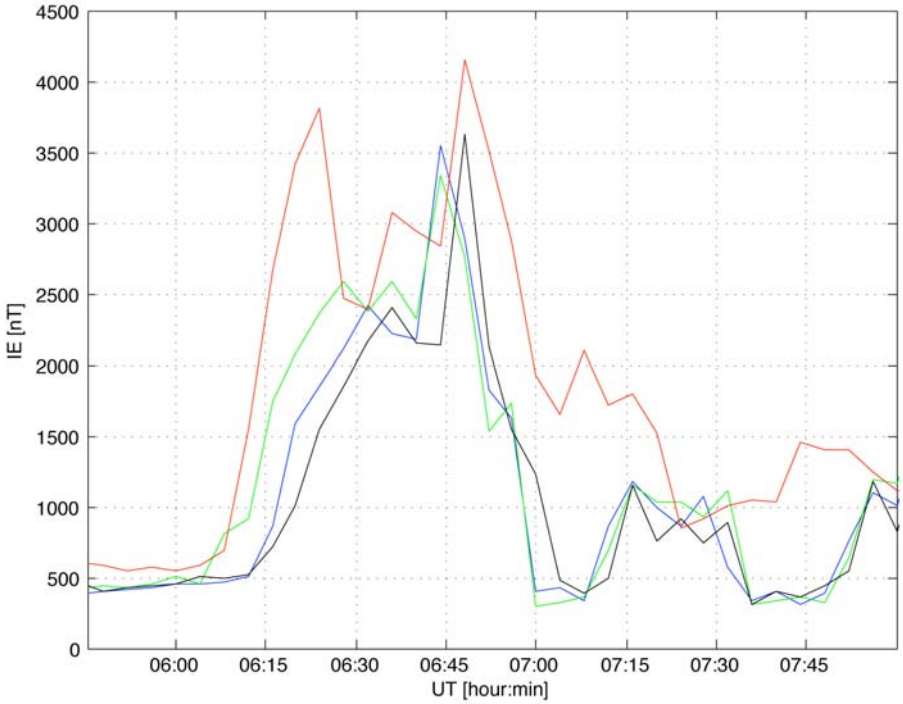

Figure 7. The *IE* index computed from the magnetic field measured at or modeled to Greenland and IMAGE magnetometer array station locations shown in Figure 4. Red line indicates the observed *IE*. The black line indicates modeled *IE* obtained using the simple convection delay, the blue line indicates modeled *IE* obtained using the phase planes with the stabilization, and the green line shows modeled *IE* obtained by using the *Weimer and King* [2008] setup. The time is UT hours of 29 October 2003.

only one free parameter. This is obviously a very appealing feature of the introduced approach that may provide an advantage over earlier minimum variance-based propagation methods when used in a real-time calculations setting.

[27] Both the introduced stabilized phase plane method and the phase plane–based setup by *Weimer and King* [2008] along with the simple convection delay propagation technique were applied for the period of 24 October to 1 November 2003 and the three propagated solar wind data sets were used as input to a global MHD model. The MHD model output was then used to compute the ground magnetic field and GIC fluctuations and these were compared to the observed magnetic field and to GIC computed by using the observed magnetic field. The results of the comparisons indicated that phase plane–based propagation methods did provide some improvements in timing of the modeled magnetic field and GIC fluctuations, the *Weimer and King* [2008] setup being able to accurately reproduce the start time of the large disturbances in the beginning of the Halloween storm events. However, the improvements were not systematic and could not be detected in the statistical analyses of the generated time series.

[28] The question remains: should one adopt phase plane–based solar wind propagation techniques to improve the accuracy of the real-time space weather forecasts? The study at hand indicates that the answer is twofold. On one hand, as was seen in Sections 3 and 4 in agreement with *Weimer et al.* [2002, 2003] and *Weimer and King* [2008], the techniques can provide quantifiable improvement to the accuracy of the solar wind propagation. On the other hand, the improvements identified in this study were quite modest. In fact, when the solar wind information was passed through the global MHD-based modeling chain to obtain the ground magnetic field and GIC, the improvement became statistically insignificant. One thus arrives at the following conclusion, which is similar to that by *Mailyan et al.* [2008]. In detailed and controlled studies it may be beneficial to use phase plane–based solar wind propagation techniques in the optimization of the timing associated with the propagated solar wind fluctuations. However, in lead time critical real-time space weather applications it may be difficult to justify the extra processing associated with the techniques when weighing the obtained improvement in the modeling accuracy against the possible lost lead time.

[29] Another question of interest is whether the introduced solar wind propagation method provides improve-

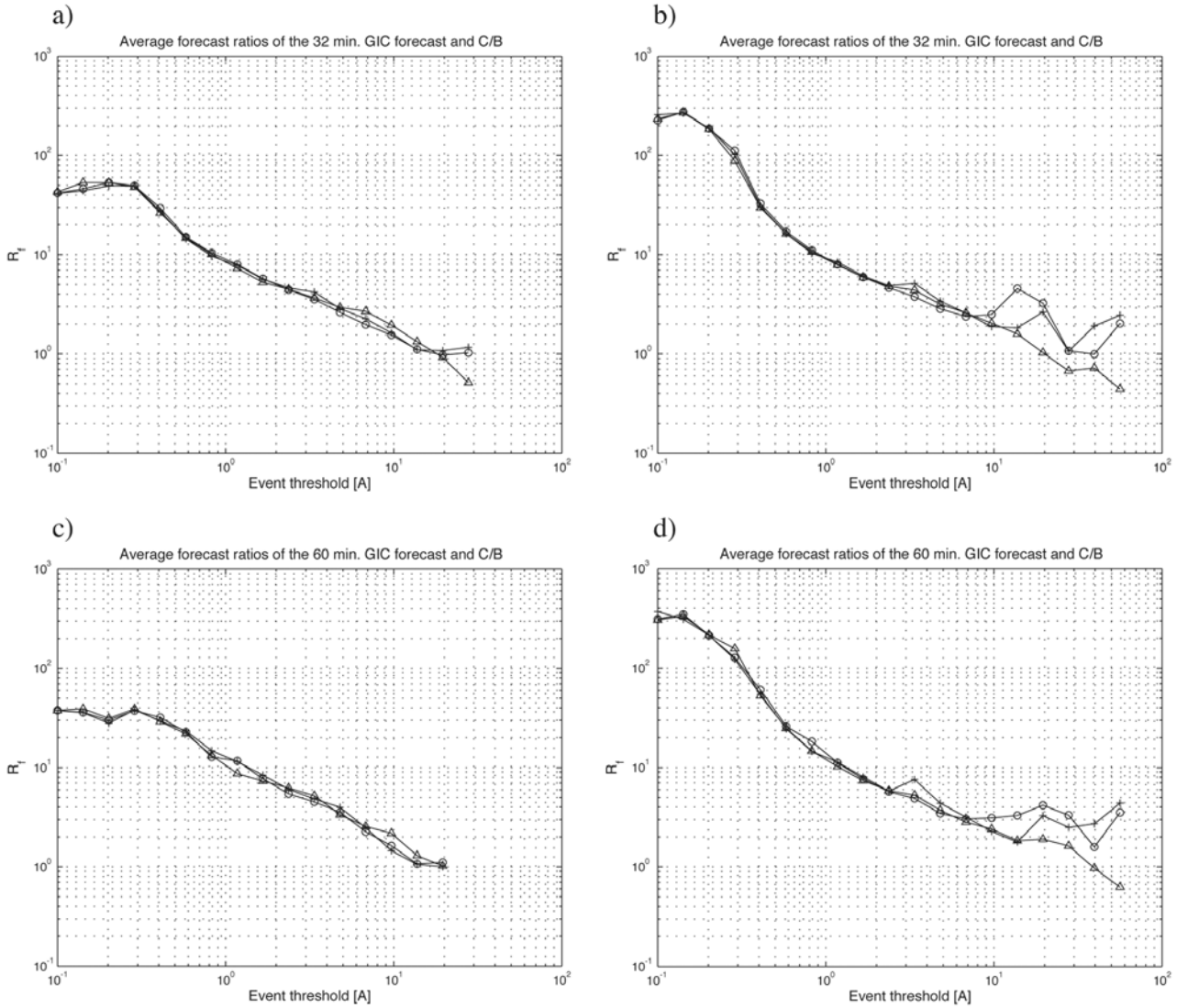

Figure 8. The forecast ratios of the GIC predictions obtained by applying the simple convection delay (triangles), the phase planes with stabilization (plusses), and the *Weimer and King* [2008] setup (circles). (a) The data was analyzed in nonoverlapping 32 minute long forecast windows. (b) The data was analyzed in overlapping 32 minute long forecast windows. (c) The data was analyzed in nonoverlapping 60 minute long forecast windows. (d) The data was analyzed in overlapping 60 minute long forecast windows. See the text and *Pulkkinen et al.* [2007] for details.

ment over the minimum variance-based setup by *Weimer and King* [2008]? It was seen that the *Weimer and King* [2008] setup provided a more accurate estimate for the start time of the Halloween storm events. This is an indication that the new method may be inferior, for example, in situations involving fast changes in the phase plane orientation, which are to some extent damped by the stabilization method. However, the two methods were seen to provide equal performance from the statistical viewpoint for the studied time periods. Although more definite conclusions will require analysis of a large collection of interplanetary discontinuities, it is thus argued that for studies involving propagation of individual discontinuity events, such as the ones studied by *Mailyan et al.* [2008], the *Weimer and King* [2008] setup may be able to provide more accurate timing. On the other hand, in real-time space weather applications involving a treatment of continuous data streams, the new method with smaller number of free parameters to adjust may be preferable.

[30] Finally, it is noted that although the phase plane–based solar wind propagation techniques when used in connection with the real-time global MHD-based modeling of the ground magnetic field and GIC fluctuations did not improve the modeling accuracy from the statistical

viewpoint for the studied time period, this does not necessarily mean that the modeling accuracy cannot be improved in other types of space weather–related applications. The MHD-based modeling carried out in this paper contains a number of sources for inaccuracy such as kinetic effects missing from the MHD approximation in the inner magnetosphere and in the plasma sheet, inaccuracies in the upstream boundary conditions thus being only one aspect of the modeling process. Consequently, modest improvement in the upstream boundary conditions may be obliterated by the other sources of inaccuracy in the modeling carried out here.

Appendix A: Mathematical Identities for Constrained Minimum Variance Analysis

[31] First the vectors and the matrices used below are defined. The three vector components of the magnetic field time series $\mathbf{B}(t_j)$ (j = 1,.., N where N is the analysis window length) are stored columnwise into a $3 \times N$ size matrix $\mathbf{X}$. $\mathbf{e}_b$ denotes a unit vector in the direction of the mean magnetic field, i.e.,

$$(e_b^1\ e_b^2\ e_b^3)^T = \mathbf{e}_b = \frac{\langle \mathbf{X} \rangle}{\sqrt{\langle \mathbf{X} \rangle^T \langle \mathbf{X} \rangle}} \tag{A1}$$

where T denotes transpose and $\langle . \rangle$ denotes mean taken over rows of $\mathbf{X}$. A projection operator is then defined as

$$\mathbf{P} = \mathbf{1} - \mathbf{e}_b \mathbf{e}_b^T \tag{A2}$$

where $\mathbf{1}$ is a 3×3 identity matrix. $\mathbf{P}$, which is identical to the operator identified by *Sonnerup and Scheible* [1998], projects vector that it operates on to a plane perpendicular to $\mathbf{e}_b$. It can be verified that the projection has the properties

$$\mathbf{P}^2 = \mathbf{P} = \mathbf{P}^T \tag{A3}$$

Note also that since the determinant of the operator vanishes, its inverse operator does not exist.

[32] The task is to find a constrained minimum variance coordinate system, i.e., here a system that is perpendicular to $\mathbf{e}_b$. To do this, the data is first projected to a plane perpendicular to $\mathbf{e}_b$ by computing

$$\mathbf{X}_\perp = \mathbf{P}\mathbf{X} \tag{A4}$$

Note that $\mathbf{X}_\perp$ has by definition zero mean. Also, as the projection $\mathbf{P}$ of the mean $\langle \mathbf{X} \rangle$ vanishes, the expression (A4) is equivalent to the projection of the centered data matrix (mean subtracted from the data) $\tilde{\mathbf{X}}$, i.e.,

$$\mathbf{X}_\perp = \mathbf{P}\mathbf{X} = \mathbf{P}\tilde{\mathbf{X}} \tag{A5}$$

The covariance matrix for the projected data is then

$$\mathbf{P}\mathbf{X}(\mathbf{P}\mathbf{X})^T = \mathbf{P}\mathbf{X}\mathbf{X}^T\mathbf{P}^T = \mathbf{P}\mathbf{Q}\mathbf{P}^T = \mathbf{P}\tilde{\mathbf{Q}}\mathbf{P}^T = \mathbf{P}\tilde{\mathbf{X}}\tilde{\mathbf{X}}^T\mathbf{P}^T \tag{A6}$$

where $\mathbf{Q}$ and $\tilde{\mathbf{Q}}$ are the covariance matrices of the original and the centered data, respectively. The constrained minimum variance analysis that searches for a coordinate system minimizing the covariance between different vector components of the time series amounts to diagonalizing expressions in equation (A6). The matrix $\mathbf{P}\mathbf{Q}\mathbf{P}^T$ is diagonalized by a matrix composed of eigenvectors $\mathbf{v}_i$ (i = 1, 2, 3) of the equation

$$\mathbf{P}\mathbf{Q}\mathbf{P}^T\mathbf{v}_i = \mathbf{P}\tilde{\mathbf{Q}}\mathbf{P}^T\mathbf{v}_i = \lambda_i \mathbf{v}_i \tag{A7}$$

where λ_i are the eigenvalues. Vectors $\mathbf{v}_i$, called also the principal components, form the orthogonal coordinate system that minimizes the data covariance perpendicular to $\mathbf{e}_b$.

[33] From equations (A4)–(A7) it is seen that the two approaches a) solving of the eigenvalue equation (A7) for $\mathbf{P}\tilde{\mathbf{Q}}\mathbf{P}^T$ as discussed by *Haaland et al.* [2006] and b) minimum variance analysis of $\mathbf{X}_\perp$, i.e., magnetic field perpendicular to $\mathbf{e}_b$ as discussed by *Bargatze et al.* [2005, 2006], are mathematically equivalent, which was observed numerically by *Bargatze et al.* [2006]. The normal of the phase plane $\mathbf{n}$ corresponds to $\mathbf{v}_i$ associated with the intermediate eigenvalue of equation (A7). The approach b) above is used in this paper and the eigenvalue equation is solved by using the singular value decomposition.

[34] It should be noted that while the treatment above uses only the magnetic field fluctuations to determine the orientation of the discontinuity, in principle also the plasma measurements can be utilized to supplement the minimum variance analysis. *Sonnerup et al.* [2006] describe a generic approach in which both the magnetic field and the plasma observations are used in the determination of the discontinuities. The central idea of their approach is that a generic conservation law leads to the diagonalization of a modified covariance matrix $\mathbf{Q}$ (note that the mathematical equivalence shown above is not valid for these more general forms of $\mathbf{Q}$). As was pointed out by *Bargatze et al.* [2006], these techniques are applicable also to the solar wind propagation problem. It is also noted that *Weimer and King* [2008] [see also *Mailyan et al.*, 2008] suggest the usage of the "cross-product method" where cross products of the average magnetic fields on different sides of the discontinuities are used to determine the phase plane, to supplement the determination of the minimum variance-based phase planes. However, as no new information in the form of additional data is introduced, it is not perfectly clear if possible small improvements in the accuracy justify the introduction of new unknown free parameters associated with the cross-product method to the calculations.

[35] **Acknowledgments.** Ari Viljanen of Finnish Meteorological Institute and Jürgen Waterman of Danish Meteorological Institute are acknowledged for providing the IMAGE and Greenland magnetometer array data, respectively, utilized in this study. R. Skoug is greatly acknowledged for providing the ACE data for the Halloween storm event. Complex image method software by A. Viljanen was used in this work. The simulations carried out for this work were done at the Community Coordinated Modeling Center (CCMC) operated at NASA Goddard Space Flight Center. The authors gratefully acknowledge researchers at the Center for Space Environment Modeling, University of Michigan who developed and provided BATS-R-US for community usage at CCMC. The authors also wish to acknowledge the rest of the CCMC staff for their generous support throughout the work discussed in the paper.

References

Bargatze, L. F., R. L. McPherron, J. Minamora, and D. Weimer (2005), A new interpretation of Weimer et al.'s solar wind propagation delay technique, *J. Geophys. Res.*, *110*, A07105, doi:10.1029/2004JA010902.

Bargatze, L. F., R. L. McPherron, J. Minamora, and D. Weimer (2006), Reply to comment by Haaland et al. on "A new interpretation of Weimer et al.'s solar wind propagation delay technique", *J. Geophys. Res.*, *111*, A06103, doi:10.1029/2005JA011557.

Boteler, D. H., R. J. Pirjola, and H. Nevanlinna (1998), The effects of geomagnetic disturbances on electrical systems at the Earth's surface, *Adv. Space Res.*, *22*, 17–27.

Haaland, S., G. Paschmann, and B. U. Ö. Sonnerup (2006), Comment on "A new interpretation of Weimer et al.'s solar wind propagation delay technique" by Bargatze et al., *J. Geophys. Res.*, *111*, A06102, doi:10.1029/2005JA011376.

Mailyan, B., C. Munteanu, and S. Haaland (2008), What is the best method to calculate the solar wind propagation delay?, *Ann. Geophys.*, *26*, 2383–2394.

Molinski, T. (2002), Why utilities respect geomagnetically induced currents, *J. Atmos. Sol. Terr. Phys.*, *64*, 1765–1778.

Pirjola, R., and A. Viljanen (1998), Complex image method for calculating electric and magnetic fields produced by an auroral electrojet of finite length, *Ann. Geophys.*, *16*, 1434–1444.

Pulkkinen, A., M. Hesse, M. Kuznetsova, and L. Rastätter (2007), First-principles modeling of geomagnetically induced electromagnetic fields and currents from upstream solar wind to the surface of the Earth, *Ann. Geophys.*, *25*, 881–893.

Skoug, R. M., J. T. Gosling, J. T. Steinberg, D. J. McComas, C. W. Smith, N. F. Ness, Q. Hu, and L. F. Burlaga (2004), Extremely high speed solar wind: 29–30 October 2003, *J. Geophys. Res.*, *109*, A09102, doi:10.1029/2004JA010494.

Sonnerup, B. U. Ö., and M. Scheible (1998), Minimum and maximum variance analysis, in *Analysis Methods for Multi-spacecraft Data*, edited by G. Paschmann and P. W. Daly, *ISSI SR-001*, pp. 185–220, ESA Publ. Div., Noordwijk, Netherlands.

Sonnerup, B. U. Ö., S. Haaland, G. Paschmann, M. W. Dunlop, H. Rème, and A. Balogh (2006), Orientation and motion of a plasma discontinuity from single-spacecraft measurements: Generic residue analysis of Cluster data, *J. Geophys. Res.*, *111*, A05203, doi:10.1029/2005JA011538.

Weimer, D. R., and J. H. King (2008), Improved calculations of interplanetary magnetic field phase front angles and propagation time delays, *J. Geophys. Res.*, *113*, A01105, doi:10.1029/2007JA012452.

Weimer, D. R., D. M. Ober, N. C. Maynard, W. J. Burke, M. R. Collier, D. J. McComas, N. F. Ness, and C. W. Smith (2002), Variable time delays in the propagation of the interplanetary magnetic field, *J. Geophys. Res.*, *107*(A8), 1210, doi:10.1029/2001JA009102.

Weimer, D. R., D. M. Ober, N. C. Maynard, M. R. Collier, D. J. McComas, N. F. Ness, C. W. Smith, and J. Watermann (2003), Predicting interplanetary magnetic field (IMF) propagation delay times using the minimum variance technique, *J. Geophys. Res.*, *108*(A1), 1026, doi:10.1029/2002JA009405. (Correction, *J. Geophys. Res.*, *109*, A12104, doi:10.1029/2004JA010691, 2004.)

A. Pulkkinen and L. Rastätter, NASA Goddard Space Flight Center, Code 674, Greenbelt, MD 20771, USA. (antti.a.pulkkinen@nasa.gov; lutz.rastaetter@nasa.gov)